Original Contribution

Noninvasive Assessment of Oxygen Extraction Fraction in Chronic Ischemia Using Quantitative Susceptibility Mapping at 7 Tesla

Ikuko Uwano, PhD; Kohsuke Kudo, MD, PhD; Ryota Sato, MS; Kuniaki Ogasawara, MD, PhD; Hiroyuki Kameda, MD; Jun-ichi Nomura, MD; Futoshi Mori, PhD; Fumio Yamashita, PhD; Kenji Ito, PhD; Kunihiro Yoshioka, MD, PhD; Makoto Sasaki, MD, PhD

Background and Purpose—The oxygen extraction fraction (OEF) is an effective metric to evaluate metabolic reserve in chronic ischemia. However, OEF is considered to be accurately measured only when using positron emission tomography (PET). Thus, we investigated whether OEF maps generated by magnetic resonance quantitative susceptibility mapping (QSM) at 7 Tesla enabled detection of OEF changes when compared with those obtained with PET.

Methods—Forty-one patients with chronic stenosis/occlusion of the unilateral internal carotid artery or middle cerebral artery were examined using 7 Tesla-MRI and PET scanners. QSM images were obtained from 3-dimensional T2*-weighted images, using a multiple dipole-inversion algorithm. OEF maps were generated based on susceptibility differences between venous structures and brain tissues on QSM images. OEF ratios of the ipsilateral middle cerebral artery territory against the contralateral side were calculated on the QSM-OEF and PET-OEF images, using an anatomic template.

Results—The OEF ratio in the middle cerebral artery territory showed significant correlations between QSM-OEF and PET-OEF maps (r=0.69; P<0.001), especially in patients with a substantial increase in the PET-OEF ratio of 1.09 (r=0.79; P=0.004), although showing significant systematic biases for the agreements. An increased QSM-OEF ratio of >1.09, as determined by receiver operating characteristic analysis, showed a sensitivity and specificity of 0.82 and 0.86, respectively, for the substantial increase in the PET-OEF ratio. Absolute QSM-OEF values were significantly correlated with PET-OEF values in the patients with increased PET-OEF.

Conclusions—OEF ratios on QSM-OEF images at 7 Tesla showed a good correlation with those on PET-OEF images in patients with unilateral steno-occlusive internal carotid artery/middle cerebral artery lesions, suggesting that noninvasive OEF measurement by MRI can be a substitute for PET. **(*Stroke*. 2017;48:00-00. DOI: 10.1161/STROKEAHA.117.017166.)**

Key Words: carotid artery, internal ■ cerebrovascular disorders ■ magnetic resonance imaging ■ middle cerebral artery ■ positron-emission tomography

Patients with severe hemodynamic ischemia termed as misery perfusion, which can be identified by an increased oxygen extraction fraction (OEF),[1] have a high risk of stroke recurrence and embolic complications during surgery.[2,3] OEF can be directly measured only by $^{15}O_2$-positron emission tomography (PET), which is considered the gold standard.[4] However, PET involves several disadvantages, such as radiation exposure, invasiveness, including arterial blood sampling, long examination times, a limited number of clinically available scanners, and lower spatial and temporal resolutions.

Recently, several approaches have attempted to measure OEF using MRI techniques.[5] In general, these techniques used blood oxygen level–dependent (BOLD) effects induced by differences in magnetic susceptibility between oxy- and deoxy-hemoglobin to quantify oxygenation in venous structures and brain parenchyma. Some of these attempted to obtain OEF values and changes by cerebrovascular challenges, such as O_2/CO_2 inhalation, hyperventilation, caffeine, acetazolamide, and sedatives.[6–11] To calculate OEF values in a resting state, however, these techniques need complex paradigms and experimental procedures that may be unavailable in clinical practice, particularly for patients with stroke or respiratory disorders. Another approach is OEF measurement without any challenges, which includes T2* or T2' relaxation measurements, termed as the quantitative BOLD,[12,13] T2 relaxation measurement using a spin-tagging technique,[14,15]

Received January 12, 2017; final revision received April 18, 2017; accepted May 30, 2017.

From the Division of Ultrahigh Field MRI, Institute for Biomedical Sciences (I.U., K.K., H.K., F.M., F.Y., K.I., M.S.), Department of Neurosurgery (K.O., J.N.), and Department of Radiology (K.Y.), Iwate Medical University, Japan; Department of Diagnostic and Interventional Radiology, Hokkaido University Hospital, Sapporo, Japan (K.K., H.K.); and Research and Development Group, Hitachi Ltd, Tokyo, Japan (R.S.).

Correspondence to Ikuko Uwano, PhD, Division of Ultrahigh Field MRI, Institute for Biomedical Sciences, Iwate Medical University, 2-1-1 Nishitokuta, Yahaba, Iwate 028-3694, Japan. E-mail uwano@iwate-med.ac.jp

Stroke **is available at http://stroke.ahajournals.org** **DOI: 10.1161/STROKEAHA.117.017166**

and phase difference measurement.[16] These methods enabled noninvasive estimation of OEF values in healthy subjects, as well as in patients with chronic ischemia and other neurological disorders.[17–21] However, the techniques are not commonly available in clinical practice in many institutes because novel scanning sequences dedicated for this purpose are needed. Moreover, the aforementioned studies performed no direct comparisons with superior O_2-PET, which is considered the gold standard to measure OEF. Hence, the availabilities, reliabilities, and accuracies of the MRI-based OEF measurement methods remain unclear, particularly in patients with cerebrovascular diseases.

Quantitative susceptibility mapping (QSM) is a post-processing technique for quantifying magnetic susceptibility of venous structures and brain parenchyma from T2*-weighted magnitude/phase images that can be easily obtained by commercial scanners. A recent study introduced a noninvasive OEF measurement method based on the QSM technique and demonstrated that OEF changes in patients with unilateral chronic steno-occlusive disease showed good correlations with those obtained by PET.[22] However, absolute OEF values and changes in the affected cerebral hemisphere tended to be underestimated presumably because of insufficient BOLD-related signal changes in minute venous structures at 3 Tesla (3T) and suboptimal post-processing algorithms. Thus, in this study, we attempted to investigate whether QSM-OEF maps obtained with a 7 Tesla (7T) scanner, which has profound susceptibility effects, and optimized post-processing techniques can readily estimate OEF changes in patients with major cerebrovascular steno-occlusive disease and can accurately detect misery perfusion when compared with OEF maps obtained by PET.

Methods

Subjects

From July 2012 to January 2016, 41 patients with chronic steno-occlusive disease of unilateral major cerebral arteries, which were evaluated by pre-operative imaging diagnosis using digital subtraction angiography or magnetic resonance angiography in our hospital, were prospectively recruited according to the following criteria: those who have unilateral occlusion or stenosis of the internal carotid artery (ICA) or middle cerebral artery (MCA; ICA stenosis, ≥70% based on The North American Symptomatic Carotid Endarterectomy Trial criteria[23]; MCA stenosis, ≥50% based on the Trial of Cilostazol in Symptomatic Intracranial Arterial Stenosis study criteria[24]) with no apparent cortical infarct in the MCA territory and those who were eligible for examinations with both 7T-MRI and PET. The details of the patient characteristics were as follows: 28 men and 13 women; age range, 29 to 82 years (median, 64 years); 19 patients with ICA occlusion, 3 with ICA stenosis, 8 with MCA occlusion, and 11 with MCA stenosis; 37 symptomatic and 4 asymptomatic patients. These patients underwent both MRI and PET scans with an interval of 2 to 24 days (mean, 4.6 days).

All examinations were performed after obtaining the approval of the institutional ethics committee (H23-45), and a written informed consent was obtained from all participants.

Imaging Protocol

We used a 7T-MRI scanner (Discovery MR950, GE Healthcare, Milwaukee, WI) with quadrature transmission and 32-channel receive head coils. Source data of QSM were obtained using a 3-dimensional spoiled gradient recalled acquisition technique with the following scanning parameters: repetition time, 30 ms; echo time, 15 ms; flip angle, 20°; field of view, 256 mm; acquisition matrix size, 512×256; slice thickness, 2 mm; number of slices, 160; reconstruction voxel size after zero-fill interpolation, 0.5 mm^3; and scan time, 3 minutes 25 seconds. The sections were set in the orthogonal axial plane from the level of the superior cerebellar peduncle to high convexity. Magnitude as well as real/imaginary phase images were regenerated from this acquisition. Structural images including T2-weighted images and magnetic resonance angiography were also obtained.

A PET study was performed using a PET/computed tomographic scanner (SET-3000GCT/M, Shimadzu Corp, Kyoto, Japan) with the inhalation technique of $^{15}O_2$. The scanner was operated in a static scan mode with dual-energy window acquisition for scatter correction, the coincidence time window of 10 ns, axial field of view of 256 mm, and the full width at half maximum for in-plane and axial spatial resolutions of 3.5 mm and 4.2 mm, respectively. The subjects continuously inhaled superior O_2 (1480 MBq) through a mask for 5 minutes, followed by a single breath of $C^{15}O$ (444 MBq). The image was reconstructed using the ordered subset expectation maximization algorithm. OEF maps were calculated using the steady-state method with correction by cerebral blood volume.[25]

Post-Processing

QSM images were generated from the source images using an in-house program with a multiple dipole-inversion combination with k-space segmentation[26] and regularization enabled sophisticated harmonic artifact reduction for phase data[27] methods. We then applied a 2-dimensional Gaussian low-pass filter with a kernel size of 60% of the total image power in each section to extract iron deposition in deep nuclei, hemosiderin deposition, dural sinuses, and large venous structures, as well as a 2-dimensional Gaussian high-pass filter of 2% to extract small venous structures. Subsequently, small venous structures were determined by multiplying the Gaussian high-pass filter–processed binary images and the logical negations of Gaussian low-pass filter–processed binary images under the threshold for binarization of > +2 SDs.

The OEF maps with voxels-of-interest of 25 mm^3 were generated from the processed QSM images according to a previous study.[22] In brief, the susceptibility difference between venous structures and surrounding brain tissues, $\Delta\chi$, is expressed by the following equation:

$$\Delta\chi = \Delta\chi_{do} \times Hct \times (1 - Y_v) \times \frac{1}{Pv} \quad (1)$$

where $\Delta\chi_{do}$ is the difference in the susceptibility per unit hematocrit between fully deoxygenated and fully oxygenated blood (we used 0.18 ppm [cgs]),[28] Hct is hematocrit (we used 0.45), Y_v is venous oxygen saturation, and Pv is a correction factor for partial volume effects that was defined as ≈7.0 according to the previous study.[22] However, OEF is defined as $(Y_a - Y_v)/Y_a$, where Y_a is arterial oxygen saturation and can be estimated as $1–Y_v$ under usual conditions in which Y_a is ≈100%.[29] Hence, OEF can be calculated with the following equation:

$$OEF = \frac{\Delta\chi \times Pv}{\Delta\chi_{do} \times Hct} \quad (2)$$

Image Analyses

Using Statistical Parametric Mapping 12 (Wellcome Department of Imaging Neuroscience, University College London, UK),[30] PET-OEF images that were coregistered to QSM source images, as well as QSM-OEF images after Gaussian smoothing (σ=10 pixel), were warped to Montreal Neurological Institute coordinates. The OEF values were then automatically measured on the sections through the lateral ventricle body and centrum semiovale; that is, z coordinate of 30 to 75 mm, using an image analysis program (ITK-SNAP, www.itksnap.org)[31] with the region of interest (ROI) of MCA territory (a combined area of pre-central, central, parietal, and angular segments) provided by 3-dimensional stereotaxic ROI template (Figure 1).[32,33] Mean OEF values were calculated for each cerebral hemisphere, and OEF ratios of the affected hemisphere against the contralateral one were obtained.

The correlations of the OEF values of the MCA ROIs, as well as OEF ratios of affected/nonaffected hemispheres between QSM and PET, were examined in all the patients and those with/without the substantial increase in PET-OEF ratios (>1.09, according to a previous study[33]) using Pearson correlation coefficient and linear regression analysis. Bland–Altman analysis was performed to examine agreements for the OEF ratios between QSM and PET in the patients with/without increased OEF. In addition, receiver operating characteristic analysis was performed to determine the sensitivity and specificity of QSM-OEF ratios for the substantial increase in PET-OEF ratios. The cut-off value of the QSM-OEF ratio was determined using Youden index. The OEF values of the ROIs were compared between the hemispheres using a Wilcoxon signed-rank test. The OEF ratios were compared between the symptomatic and asymptomatic patients using a Mann–Whitney *U* test and between the patients with occlusion/stenosis of ICA/MCA using a Steel-Dwass test. Correlations between the QSM-PET difference in the OEF ratios and degree of MCA stenosis were examined using Pearson correlation coefficient. The cut-off α level used was 0.05.

Results

Two patients were excluded because of profound metallic artifacts and severe motion artifacts. The remaining 39 patients (26 men and 13 women; age range, 29–82 years [median, 64 years]; 18 ICA occlusion, 3 ICA stenosis, 8 MCA occlusion, and 10 MCA stenosis; 35 symptomatic and 4 asymptomatic patients) were eligible for further analyses. We successfully obtained QSM-OEF images that appeared visually comparable with the corresponding PET-OEF images (Figure 1).

Both QSM-OEF and PET-OEF values in the affected hemisphere (range [median], 40.0%–64.4% [50.0%] and 32.4%–70.2% [46.8%], respectively) were significantly higher than those in the contralateral hemisphere (39.2%–62.1% [47.6%] and 30.5%–59.2% [44.2%]; P=0.004 and P<0.001, respectively). In addition, there was a significant correlation of the OEF values in both hemispheres between the QSM and PET in 11 patients with a substantial increase in PET-OEF ratio >1.09 (r=0.64; P=0.001; y=0.41x+29.2) although there was no significant correlation in the remaining 28 patients (r=−0.19; P=0.17; y=−0.12x+54.2; Figure 2).

Regarding the OEF ratio of the affected hemisphere against the contralateral side, a good correlation was found between the QSM-OEF maps and the PET-OEF maps (r=0.69; P<0.001; y=0.53x+0.48; Figure 3). In the patients with an increased PET-OEF ratio, an excellent correlation was observed between the images (r=0.79; P=0.004; y=0.53x+0.47), whereas there was no significant correlation in other patients (r=0.21; P=0.27). Bland–Altman analysis between QSM-OEF and PET-OEF ratios showed that, although most all of the values are within mean±2SD, the constant bias was observed in the patients with increased PET-OEF ratios (mean difference, −0.11; 95% confidence interval, −0.17 to −0.06) while the proportional bias was observed in the patients with maintained PET-OEF ratios (slope of regression equation, 1.17 [P<0.001]; Figure 4), indicating the suboptimal agreements.

There were no significant differences in the QSM-OEF and PET-OEF values between symptomatic and asymptomatic patients (P=0.94 and 0.47, respectively; Mann–Whitney *U* test) and among the patients with occlusion/stenosis of ICA/MCA (P=0.11–1.00 and 0.08–1.00, respectively; Steel-Dwass test). The QSM-PET differences in the OEF ratios showed no significant correlations with the degree of stenosis in the patients with MCA stenosis (r=0.004; P=0.99).

The receiver operating characteristic analysis showed that the area under the curve of QSM-OEF ratios against increased PET-OEF ratios was 0.85 (95% confidence interval, 0.72–0.99) and the sensitivity and specificity were 0.82 (9 of 11; 95% confidence interval, 0.48–0.98) and 0.86 (24 of 28; 95% confidence interval, 0.67–0.96), respectively, when the cut-off value was set as 1.09 (Figure 3).

Discussion

In this study, we assessed accuracies of the QSM-OEF at 7T by comparing results with PET-OEF in patients with unilateral major vessel stenosis or occlusion and revealed that the QSM-OEF ratio of the ipsilateral MCA territory against the contralateral side showed a good correlation with PET-OEF and readily discriminated patients with

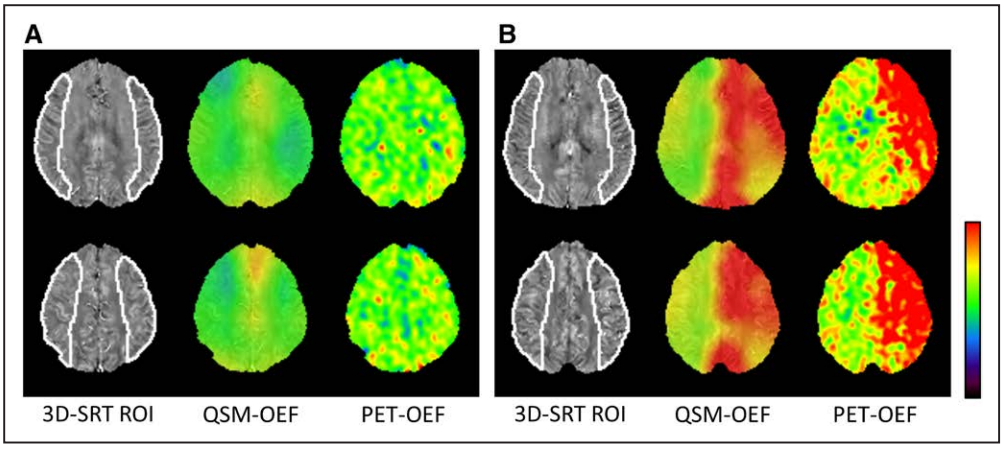

Figure 1. Oxygen extraction fraction (OEF) images of patients with chronic ischemia obtained by quantitative susceptibility mapping (QSM) and positron emission tomography (PET). **A**, A 46-year-old woman with right middle cerebral artery stenosis. OEF values showed no apparent asymmetry on QSM-OEF and PET-OEF images (OEF ratios, 1.00 and 0.96, respectively). **B**, A 74-year-old man with left internal carotid artery occlusion. OEF values of the ipsilateral hemisphere on the QSM-OEF image are evidently increased and are comparable to those on the PET-OEF image (OEF ratios, 1.35 and 1.46, respectively). 3D-SRT ROI indicates 3-dimensional stereotaxic region of interest.

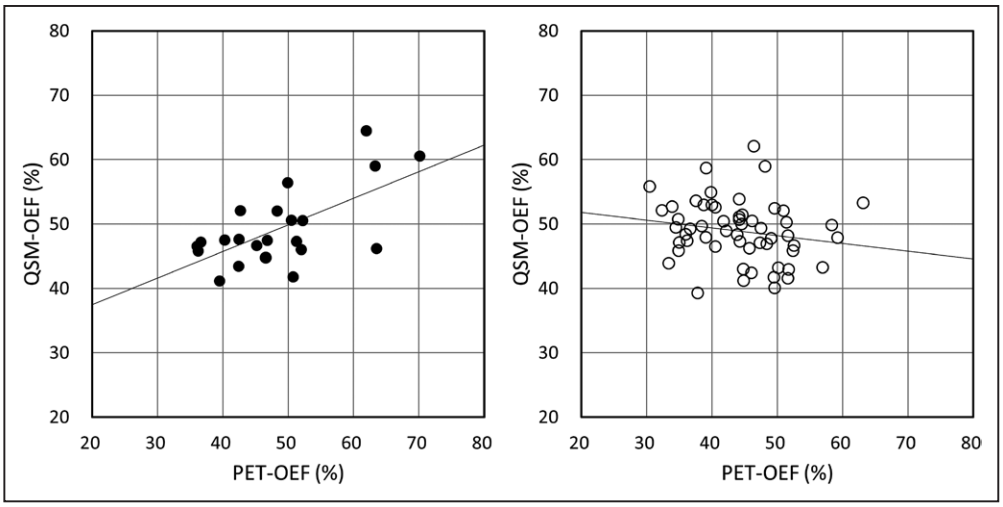

Figure 2. Absolute oxygen extraction fraction (OEF) values obtained by quantitative susceptibility mapping (QSM) and positron emission tomography (PET) in patients with unilateral internal carotid artery/middle cerebral artery stenosis/occlusion. There was a significant correlation between QSM-OEF and PET-OEF values of the bilateral hemispheres in the patients with increased PET-OEF ratios >1.09 (●; r=0.64; P=0.001) although no correlation was found in patients with preserved PET-OEF ratios (○; r=−0.19; P=0.17).

increased OEF from others. These results were comparable to those of QSM-OEF at 3T in a previous report,[22] indicating the potential use of the QSM-based OEF estimation to evaluate OEF abnormalities, including misery perfusion as a noninvasive alternative to $^{15}O_2$-PET and other invasive methods.

Various MRI approaches that share some theoretical similarities have been used for OEF estimation.[5] When compared with the methods reported previously,[6–16] the QSM-based method we used has several advantages, such as usage of conventional sequence; short acquisition time; no need for any challenge, contrast agent, or other invasive procedures; sufficient spatial resolution with whole-brain coverage; and robustness to low perfusion status, suggesting high availability in clinical practice and clinical studies for patients with cerebrovascular and other neurological disorders. However, this method highly depends on the algorithms for generating QSM images and for estimating OEF values. Several algorithms for QSM generation were proposed,[26,34–38] and they vary in terms of preservation of small venous structures, which seems crucial to obtain accurate OEF values. The software for estimating OEF values from QSM images has remained as in-house programs that need further revisions to distribute as free software programs. Further optimization of the algorithm and parameters, as well as publication of the program, is needed for wide adoption of the QSM-OEF method.

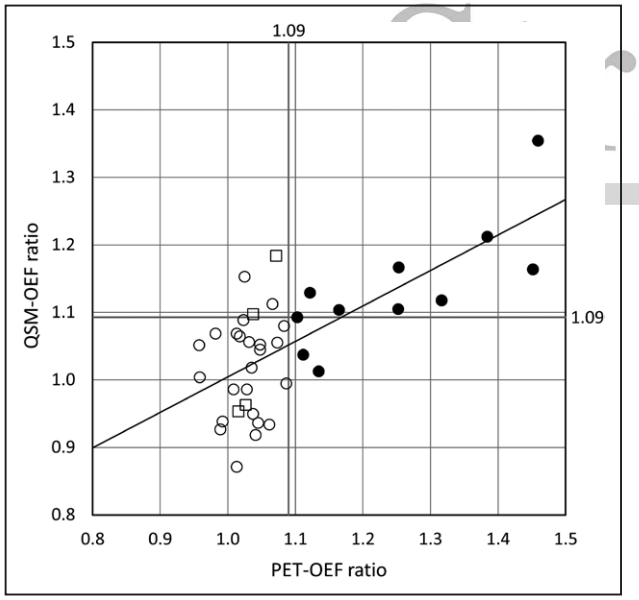

Figure 3. Oxygen extraction fraction (OEF) ratios of affected/nonaffected hemispheres obtained by quantitative susceptibility mapping (QSM) and positron emission tomography (PET) in patients with unilateral internal carotid artery/middle cerebral artery stenosis/occlusion. There is a significant correlation between QSM-OEF and PET-OEF ratios (r=0.69; P<0.001), particularly in the patients with increased PET-OEF ratios (●; r=0.79; P=0.004; regression line, y=0.53x+0.48). Horizontal and vertical solid lines indicate cut-off values of normal ranges for QSM-OEF (1.09, determined by receiver operating characteristic analysis) and for PET-OEF (1.09, taken from the previous report). □, asymptomatic patients.

In this study, we used a 7T scanner that yields profound susceptibility effects to improve accuracies for estimating OEF values. Against our expectations, however, the QSM-OEF at 7T in this study achieved only a slight improvement in terms of the correlation coefficient and the sensitivity/specificity for PET-OEF and included substantial systematic biases in terms of the agreements, when compared with that at 3T in the previous report.[22] This issue can be mainly attributed to the relatively low spatial resolution of the source images, which were comparable to that at 3T in the previous study.[22] Although the BOLD effect is much stronger at 7T than at 3T, we presumably overlooked susceptibility information of minute venous structures because of the low resolution of the images. In addition, the results can be affected by the differences in the cohorts, ROIs, and post-processing methods from the previous study.[22] Moreover, regarding the absolute OEF values, we found only a fair correlation between QSM and PET. Besides the aforementioned reasons, this issue can be partly explained by the

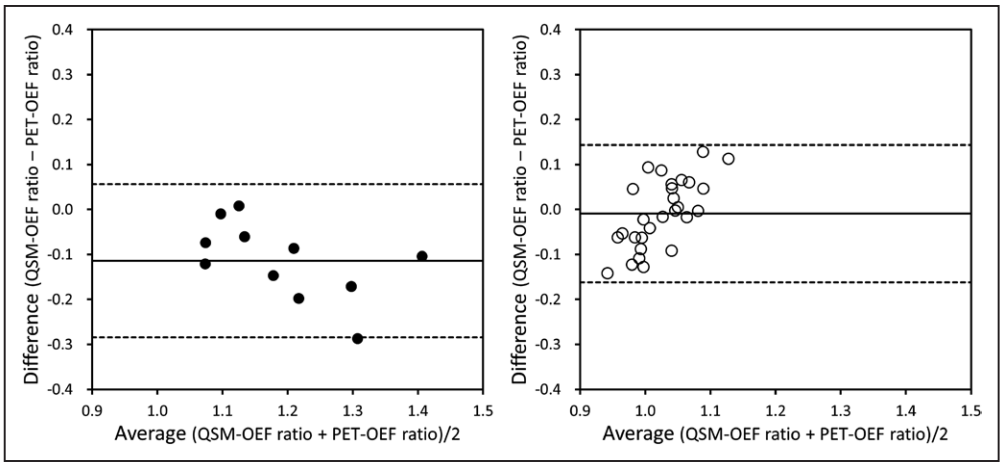

Figure 4. Agreements in oxygen extraction fraction (OEF) ratios of affected/nonaffected hemispheres obtained by quantitative susceptibility mapping (QSM) and positron emission tomography (PET) in patients with/without increased PET-OEF. Bland–Altman plots show that differences in OEF ratios between QSM and PET ranged within 95% limits of the agreement (mean±2SD; dashed lines) in almost all the patients; however, there are a constant bias in those with increased PET-OEF (●) and a proportional bias in those with preserved PET-OEF (○).

theoretical discrepancy that QSM-OEF reflects oxygenation within venous structures, whereas PET-OEF mainly reflects that within brain parenchyma. Direct comparisons between 7T and 3T images in the same patients with the identical post-processing and analysis methods are needed to clarify potential advantages of the 7T system.

We generated OEF maps only from the QSM images at resting state in this study. However, the QSM-based method can be applied for paradigms using cerebrovascular challenges, which were proposed by the previous studies.[6–10] These methods can minimize influences by paramagnetic effects because of iron deposition of deep nuclei, hemosiderin deposition, and neighboring bone/air structures, which enabled selective assessment of susceptibility changes in response to external stimuli. By using the paradigms, we may improve accuracies of OEF estimation although the availability may be compromised because of invasiveness and long examination times.

This study had several limitations. First, we performed no comparisons with clinical outcomes of the patients because of the relatively small sample size of the heterogeneous cohort. Hence, we did not fully determine the clinical significance of the method we used although we demonstrated accurate detection of substantial increases in OEF of affected cerebral hemispheres. Second, we did not compare our method with the other methods previously reported, such as paradigms using cerebrovascular challenges, T2*/T2' relaxation measurements, spin-tagging T2 relaxation measurements, and phase difference measurements. Therefore, whether the QSM-based OEF estimation is more accurate than the other methods remains unknown. Third, we did not compare OEF values between 7T and 3T or between QSM algorithms so that advantages of the 7T scanner and algorithm we used remain unclear. Furthermore, we did not examine the effects of spatial resolution of source images on OEF accuracies although we consider spatial resolution crucial even at 7T. To overcome the issues, further technical improvements and optimization, as well as prospective studies with larger sample sizes, are needed, some of which are ongoing.

Conclusions

The OEF obtained by QSM at 7T was well correlated with that obtained by $^{15}O_2$-PET in terms of the ratio of affected/nonaffected sides in patients with unilateral ICA/MCA stenoocclusive lesions and enabled accurate evaluation of the substantial OEF increase, which suggests that noninvasive OEF measurements based on the QSM technique can be used as a substitute for PET for assessment of chronic ischemia and other cerebrovascular disorders.

Sources of Funding

This work was partly supported by a Grant-in-Aid for Strategic Medical Science Research (S1491001, 2014–2018) and Grants-in-Aid for Scientific Research (grant no. 16K10798) from the Ministry of Education, Culture, Sports, Science and Technology of Japan, as well as by Grain-in-Aid from Senshin Medical Research Foundation.

Disclosures

R. Sato is an employee of Hitachi Ltd. The other authors report no conflicts.

References

1. Baron JC, Bousser MG, Rey A, Guillard A, Comar D, Castaigne P. Reversal of focal "misery-perfusion syndrome" by extra-intracranial arterial bypass in hemodynamic cerebral ischemia. A case study with 15O positron emission tomography. *Stroke*. 1981;12:454–459.
2. Grubb RL Jr, Derdeyn CP, Fritsch SM, Carpenter DA, Yundt KD, Videen TO, et al. Importance of hemodynamic factors in the prognosis of symptomatic carotid occlusion. *JAMA*. 1998;280:1055–1060.
3. Yamauchi H, Higashi T, Kagawa S, Nishii R, Kudo T, Sugimoto K, et al. Is misery perfusion still a predictor of stroke in symptomatic major cerebral artery disease? *Brain*. 2012;135(pt 8):2515–2526. doi: 10.1093/brain/aws131.
4. Baron JC, Jones T. Oxygen metabolism, oxygen extraction and positron emission tomography: historical perspective and impact on basic and clinical neuroscience. *Neuroimage*. 2012;61:492–504. doi: 10.1016/j.neuroimage.2011.12.036.
5. Christen T, Bolar DS, Zaharchuk G. Imaging brain oxygenation with MRI using blood oxygenation approaches: methods, validation, and clinical applications. *AJNR Am J Neuroradiol*. 2013;34:1113–1123. doi: 10.3174/ajnr.A3070.
6. Bulte DP, Kelly M, Germuska M, Xie J, Chappell MA, Okell TW, et al. Quantitative measurement of cerebral physiology using

respiratory-calibrated MRI. *Neuroimage*. 2012;60:582–591. doi: 10.1016/j.neuroimage.2011.12.017.
7. Wise RG, Harris AD, Stone AJ, Murphy K. Measurement of OEF and absolute CMRO2: MRI-based methods using interleaved and combined hypercapnia and hyperoxia. *Neuroimage*. 2013;83:135–147. doi: 10.1016/j.neuroimage.2013.06.008.
8. Zhang J, Liu T, Gupta A, Spincemaille P, Nguyen TD, Wang Y. Quantitative mapping of cerebral metabolic rate of oxygen (CMRO2) using quantitative susceptibility mapping (QSM). *Magn Reson Med*. 2015;74:945–952. doi: 10.1002/mrm.25463.
9. Zaitsu Y, Kudo K, Terae S, Yazu R, Ishizaka K, Fujima N, et al. Mapping of cerebral oxygen extraction fraction changes with susceptibility-weighted phase imaging. *Radiology*. 2011;261:930–936. doi: 10.1148/radiol.11102416.
10. Goodwin JA, Kudo K, Shinohe Y, Higuchi S, Uwano I, Yamashita F, et al. Susceptibility-weighted phase imaging and oxygen extraction fraction measurement during sedation and sedation recovery using 7T MRI. *J Neuroimaging*. 2015;25:575–581. doi: 10.1111/jon.12192.
11. De Vis JB, Petersen ET, Bhogal A, Hartkamp NS, Klijn CJ, Kappelle LJ, et al. Calibrated MRI to evaluate cerebral hemodynamics in patients with an internal carotid artery occlusion. *J Cereb Blood Flow Metab*. 2015;35:1015–1023. doi: 10.1038/jcbfm.2015.14.
12. An H, Lin W. Quantitative measurements of cerebral blood oxygen saturation using magnetic resonance imaging. *J Cereb Blood Flow Metab*. 2000;20:1225–1236. doi: 10.1097/00004647-200008000-00008.
13. He X, Yablonskiy DA. Quantitative BOLD: mapping of human cerebral deoxygenated blood volume and oxygen extraction fraction: default state. *Magn Reson Med*. 2007;57:115–126. doi: 10.1002/mrm.21108.
14. Lu H, Ge Y. Quantitative evaluation of oxygenation in venous vessels using T2-relaxation-under-spin-tagging MRI. *Magn Reson Med*. 2008;60:357–363. doi: 10.1002/mrm.21627.
15. Bolar DS, Rosen BR, Sorensen AG, Adalsteinsson E. QUantitative Imaging of eXtraction of oxygen and TIssue consumption (QUIXOTIC) using venular-targeted velocity-selective spin labeling. *Magn Reson Med*. 2011;66:1550–1562. doi: 10.1002/mrm.22946.
16. Fan AP, Benner T, Bolar DS, Rosen BR, Adalsteinsson E. Phase-based regional oxygen metabolism (PROM) using MRI. *Magn Reson Med*. 2012;67:669–678. doi: 10.1002/mrm.23050.
17. Xie S, Hui LH, Xiao JX, Zhang XD, Peng Q. Detecting misery perfusion in unilateral steno-occlusive disease of the internal carotid artery or middle cerebral artery by MR imaging. *AJNR Am J Neuroradiol*. 2011;32:1504–1509. doi: 10.3174/ajnr.A2523.
18. Yu L, Xie S, Xiao J, Wang Z, Zhang X. Quantitative measurement of cerebral oxygen extraction fraction using MRI in patients with MELAS. *PLoS One*. 2013;8:e79859. doi: 10.1371/journal.pone.0079859.
19. Ge Y, Zhang Z, Lu H, Tang L, Jaggi H, Herbert J, et al. Characterizing brain oxygen metabolism in patients with multiple sclerosis with T2-relaxation-under-spin-tagging MRI. *J Cereb Blood Flow Metab*. 2012;32:403–412. doi: 10.1038/jcbfm.2011.191.
20. Fan AP, Govindarajan ST, Kinkel RP, Madigan NK, Nielsen AS, Benner T, et al. Quantitative oxygen extraction fraction from 7-Tesla MRI phase: reproducibility and application in multiple sclerosis. *J Cereb Blood Flow Metab*. 2015;35:131–139. doi: 10.1038/jcbfm.2014.187.
21. Liu Z, Li Y. Cortical cerebral blood flow, oxygen extraction fraction, and metabolic rate in patients with middle cerebral artery stenosis or acute stroke. *AJNR Am J Neuroradiol*. 2016;37:607–614. doi: 10.3174/ajnr.A4624.
22. Kudo K, Liu T, Murakami T, Goodwin J, Uwano I, Yamashita F, et al. Oxygen extraction fraction measurement using quantitative susceptibility mapping: comparison with positron emission tomography. *J Cereb Blood Flow Metab*. 2016;36:1424–1433. doi: 10.1177/0271678X15606713.
23. North American Symptomatic Carotid Endarterectomy Trial. Methods, patient characteristics, and progress. *Stroke*. 1991;22:711–720.
24. Kwon SU, Cho YJ, Koo JS, Bae HJ, Lee YS, Hong KS, et al. Cilostazol prevents the progression of the symptomatic intracranial arterial stenosis: the multicenter double-blind placebo-controlled trial of cilostazol in symptomatic intracranial arterial stenosis. *Stroke*. 2005;36:782–786. doi: 10.1161/01.STR.0000157667.06542.b7.
25. Lammertsma AA, Jones T. Correction for the presence of intravascular oxygen-15 in the steady-state technique for measuring regional oxygen extraction ratio in the brain: 1. Description of the method. *J Cereb Blood Flow Metab*. 1983;3:416–424. doi: 10.1038/jcbfm.1983.67.
26. Sato R, Shirai T, Taniguchi Y, Murase T, Bito Y, Ochi H. Quantitative susceptibility mapping using the multiple dipole-inversion combination with k-space segmentation method [published online ahead of print March 27, 2017]. *Magn Reson Med Sci*. 2017. doi: 10.2463/mrms.mp.2016-0062. https://www.jstage.jst.go.jp/article/mrms/advpub/0/advpub_mp.2016-0062/_pdf.
27. Sun H, Wilman AH. Background field removal using spherical mean value filtering and Tikhonov regularization. *Magn Reson Med*. 2014;71:1151–1157. doi: 10.1002/mrm.24765.
28. Weisskoff RM, Kiihne S. MRI susceptometry: image-based measurement of absolute susceptibility of MR contrast agents and human blood. *Magn Reson Med*. 1992;24:375–383.
29. van Zijl PC, Eleff SM, Ulatowski JA, Oja JM, Uluğ AM, Traystman RJ, et al. Quantitative assessment of blood flow, blood volume and blood oxygenation effects in functional magnetic resonance imaging. *Nat Med*. 1998;4:159–167.
30. Ashburner J. SPM: a history. *Neuroimage*. 2012;62:791–800. doi: 10.1016/j.neuroimage.2011.10.025.
31. Yushkevich PA, Piven J, Hazlett HC, Smith RG, Ho S, Gee JC, et al. User-guided 3D active contour segmentation of anatomical structures: significantly improved efficiency and reliability. *Neuroimage*. 2006;31:1116–1128. doi: 10.1016/j.neuroimage.2006.01.015.
32. Takeuchi R, Matsuda H, Yoshioka K, Yonekura Y. Cerebral blood flow SPET in transient global amnesia with automated ROI analysis by 3DSRT. *Eur J Nucl Med Mol Imaging*. 2004;31:578–589. doi: 10.1007/s00259-003-1406-8.
33. Chida K, Ogasawara K, Kuroda H, Aso K, Kobayashi M, Fujiwara S, et al. Central benzodiazepine receptor binding potential and CBF images on SPECT correlate with oxygen extraction fraction images on PET in the cerebral cortex with unilateral major cerebral artery occlusive disease. *J Nucl Med*. 2011;52:511–518. doi: 10.2967/jnumed.110.084186.
34. Liu T, Spincemaille P, de Rochefort L, Kressler B, Wang Y. Calculation of susceptibility through multiple orientation sampling (COSMOS): a method for conditioning the inverse problem from measured magnetic field map to susceptibility source image in MRI. *Magn Reson Med*. 2009;61:196–204. doi: 10.1002/mrm.21828.
35. Shmueli K, de Zwart JA, van Gelderen P, Li TQ, Dodd SJ, Duyn JH. Magnetic susceptibility mapping of brain tissue in vivo using MRI phase data. *Magn Reson Med*. 2009;62:1510–1522. doi: 10.1002/mrm.22135.
36. Liu T, Liu J, de Rochefort L, Spincemaille P, Khalidov I, Ledoux JR, et al. Morphology enabled dipole inversion (MEDI) from a single-angle acquisition: comparison with COSMOS in human brain imaging. *Magn Reson Med*. 2011;66:777–783. doi: 10.1002/mrm.22816.
37. Schweser F, Sommer K, Deistung A, Reichenbach JR. Quantitative susceptibility mapping for investigating subtle susceptibility variations in the human brain. *Neuroimage*. 2012;62:2083–2100. doi: 10.1016/j.neuroimage.2012.05.067.
38. Wu B, Li W, Guidon A, Liu C. Whole brain susceptibility mapping using compressed sensing. *Magn Reson Med*. 2012;67:137–147. doi: 10.1002/mrm.23000.

Noninvasive Assessment of Oxygen Extraction Fraction in Chronic Ischemia Using Quantitative Susceptibility Mapping at 7 Tesla

Ikuko Uwano, Kohsuke Kudo, Ryota Sato, Kuniaki Ogasawara, Hiroyuki Kameda, Jun-ichi Nomura, Futoshi Mori, Fumio Yamashita, Kenji Ito, Kunihiro Yoshioka and Makoto Sasaki

Stroke. published online June 29, 2017;
Stroke is published by the American Heart Association, 7272 Greenville Avenue, Dallas, TX 75231

Print ISSN: 0039-2499. Online ISSN: 1524-4628